Journal of Power Sources 196 (2011) 1229–1234

Contents lists available at ScienceDirect

Journal of Power Sources

journal homepage: www.elsevier.com/locate/jpowsour

A membraneless microfluidic fuel cell stack

Kamil S. Salloum[a], Jonathan D. Posner[a,b,*]

[a] Mechanical Engineering, Arizona State University, Tempe, AZ 85287, United States
[b] Chemical Engineering, Arizona State University, Tempe, AZ 85287, United States

ARTICLE INFO

Article history:
Received 13 July 2010
Received in revised form 24 August 2010
Accepted 24 August 2010
Available online 21 September 2010

Keywords:
Microfluidic fuel cell
Membraneless fuel cell
Flow battery
Fuel utilization
Reactant recycling
Stacked fuel cell

ABSTRACT

A membraneless microfluidic fuel cell stack architecture is presented that reuses reactants from one cell to a subsequent one, analogous to PEMFC stacks. On-chip reactant reuse improves fuel utilization and power densities relative to single cells. The reactants flow separately through porous electrodes and interface with a non-reacting and conductive electrolyte which maintains their separation. The reactants remain separated downstream of the interface and are used in subsequent downstream cells. This fuel cell uses porous carbon for electrocatalysts and vanadium redox species as reactants with a sulfuric acid supporting electrolyte. The overall power density of the fuel cell increases with reactant flow rate and decreasing the separating electrolyte flow rate. The peak power, maximum fuel utilization, and efficiency nearly double when electrically connecting the cells in parallel.

© 2010 Elsevier B.V. All rights reserved.

1. Introduction

The rapid advancement of portable electronic devices has significantly increased their power demands [1–3]. Current state of the art battery technologies are a major contributor to the overall weight and size of the portable system due to their low energy densities. Liquid and gaseous fuels exhibit higher energy densities compared to battery systems, and offer greater flexibility in their storage, handling, and system implementation [4]. Miniaturized polymer membrane fuel cells that use fuels present a small scale and portable solution with high fuel conversion efficiency [5–14]. However, like their full scale counterparts, miniaturized fuel cells suffer from complications with membrane and electrode durability [15–22], water management at the cathode [23–25], and reactant crossover [26–29]. Such challenges increase the overall cost and maintenance and reduce the system's reliability.

More recently, micron scale membraneless fuel cells have been developed as alternative portable power sources [30–32]. Microfluidic membraneless fuel cells avoid the use of a semi-permeable membrane by leveraging laminar interfaces between the liquid streams to separate the reactants. Membraneless fuel cells offer greater flexibility with fuel and oxidant selection than membrane-based cells because they do not have the inherent crossover issues [33]. Membraneless fuel cells have been demonstrated with vanadium [31,34–36], formic acid [30,37], hydrogen saturated electrolytes [38–40], gaseous streams [40–42], peroxide [43], methanol [44,45], ethanol [46], borohydride [47], hypochlorite [48], and have been tested in both basic and acidic media [48–51].

Microfluidic fuel cells have primarily relied on parallel flowing laminar streams of fuel and oxidant [32,52]. The parallel flow design requires careful consideration of the development of both the viscous and concentration boundary layers, because the flow rates are linked to the power density and fuel utilization [32,33]. The power density of parallel flow fuel cells increases with increasing flow rate [32]. Higher flow rates generate higher power because they reduce the concentration boundary layer thickness at the electrodes resulting in lower mass transport losses [53,54]. The improvements in power density come at the expense of fuel utilization because the fuel and oxidant reach the end of the cell before they are consumed. Membraneless fuel cells typically exhibit higher Ohmic losses than membrane-based systems which results in lower power densities. The increased Ohmic loss is attributed to the increased electrode spacing. In co-flowing laminar streams, unreacted fuel and oxidant mix by transverse diffusion at the laminar flow interface, which results in reactant depletion [51,55,56]. For a given length of laminar flow fuel cell, diffusive mixing of the fuel and oxidant decreases with increasing flow rate because the reactants are advected downstream with greater velocity (higher effective Peclet number). Although larger flow rates result in less mixing of the streams at the interface and higher power output from the cell, the fuel and oxidant may reach the end of the cell before they are consumed, resulting in a net reduction in fuel utilization.

Various architectures have been presented to overcome the abovementioned challenges of boundary layer growth and diffusive

* Corresponding author. Tel.: +1 480 965 1799; fax: +1 480 965 1384.
E-mail address: jposner@asu.edu (J.D. Posner).

0378-7753/$ – see front matter © 2010 Elsevier B.V. All rights reserved.
doi:10.1016/j.jpowsour.2010.08.069

broadening at the interface. Kjeang et al. increased electrocatalyst surface area using sheets or stacks of graphite rods in a vanadium redox fuel cell in an effort to improve fuel utilization [34,35]. Cohen et al. introduced a planar tapered flow that delays the onset of reactant depletion to reduce wasted reactant [38]. Sun et al. introduced a parallel flowing electrolyte between the reactant streams in order to reduce reactant mixing [39]. Yoon et al. used additional downstream inlets in an effort to replenish the depletion zones at the sidewall electrodes [57]. Membraneless fuel cells have also been studied from both a computational and analytical approach to identify and characterize the relationship of flow conditions to the cell's power output and fuel utilization [58–61]. Recent membraneless fuel cell architectures show more active effort to overcome challenges with mixing and depletion of reactants. Brushett et al. [49,50] and Jayashree et al. [42,62] applied gas diffusion layers with gaseous streams to mitigate challenges with reactant mixing. Hollinger et al. used a non-selective nanoporous separator between fuel and oxidant to overcome challenges with reactant cross diffusion and mixed potentials [63]. Kjeang et al. [36] and our previous work [37] used a flow through architecture with porous electrodes that increased reaction surface area availability to increase fuel utilization at higher flow rates, and alleviate deficiencies with mass boundary layer depletion zones common in flat plate electrode designs. In our previous works we also introduced a sequential flow field where the fuel and oxidant flow in series [37], and a counter flow pattern where a non-reacting electrolyte separates the fuel and oxidant to independent outlets [64]. Both of the sequential and counter flow designs featured concise ionic interfaces where advection occurs in the direction of concentration gradients which mitigates diffusion of reactants even at low Peclet numbers. Although various fuel cell architectures as well as fuel and catalyst selection have provided improvements in power density and fuel utilization, these two figures of merit are still strongly linked to the flow rate in the system. Existing membraneless systems have failed to provide high power density and complete fuel utilization analogous to a stacked PEM membrane-based system.

In this work, we present a membraneless microfluidic fuel cell that, for the first time, enables stacking of reaction zones analogous to membrane-based fuel cell stacks. This design keeps the reactants separate and enables the reactants to be reused, increasing the fuel utilization of the cell and effectively decoupling the power density from the fuel utilization. The cell presented here integrates two reactant and electrolyte interfaces on a single fluidic chip allowing for multiple passes of the reactants. Fig. 1 shows the flow pattern in the multi-pass microfluidic fuel cell. The shortened ion exchange zone reduces reactant mixing and the non-reacting electrolyte ensures their separation. The reactants are reused at a downstream reaction zone, effectively increasing the overall interfacial area. In this manner the fuel utilization is decoupled from the flow rate which will ultimately yield higher overall power density and thermodynamic efficiency. In this flow configuration, the fuel and the oxidant are first introduced through a porous electrocatalyst. At the interface junction between the anode and the cathode, an electrolyte splits equally to direct the fuel and oxidant through independent channels leading from cell 1 into cell 2. The exact flow pattern is repeated in cell 2, and terminates with the fuel and oxidant flowing to independent outlets. Each interface is treated as an individual electrochemical cell with its own porous anode and cathode, and external contact for current sourcing.

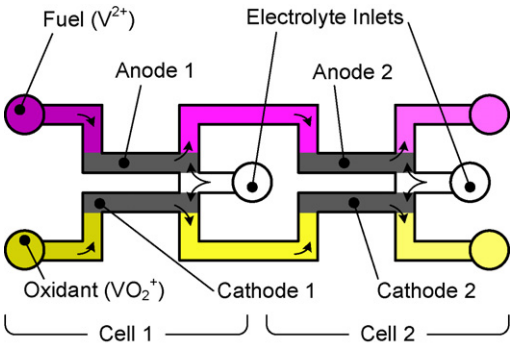

Fig. 1. Top view schematic of the multi-pass fuel cell. After reacting through the porous electrodes in cell 1, the fuel and the oxidant are redirected by an electrolyte to cell 2. Arrows represent flow direction.

The multi-pass design (i) separates the reactants throughout the device, (ii) provides a high conductivity ionic exchange zone that reduces reactant diffusive mixing, and (iii) uses porous electrocatalysts to increase available reaction surface area. This design results in an effective increase in the ionic exchange cross-sectional area by repeating interfaces, similar to a stacked PEM fuel cell architecture, exhibiting reduced reactant mixing compared to a single extended diffusive interface. It is difficult to maintain the stability of an extended interface due to an increase in downstream diffusive mixing and susceptibility to perturbations in elongated channels. Fig. 2 shows flow visualization optical micrographs of the fuel cell design cell under various ratios of the flow rate of the reactants to that of the separating electrolyte. It is preferential to use lower separating electrolyte flow rates as to not overwhelmingly dilute the reactants at each subsequent interface, and to increase the overall gravimetric power density and reduce pumping power associated with carrying a non-reacting electrolyte. The Reynolds number at each micrograph in Fig. 2 is defined as $\mathrm{Re} = UD_h/\upsilon$, where U is the average fluid velocity in the channel, D_h is the hydraulic diameter of the channel, and υ is the kinematic viscosity of the fluid. The purpose of the visualization is to investigate the onset of reactant mixing due to decreased separating electrolyte flow rate. Fig. 2D suggests that even at electrolyte flow rates of only 6% the reactant flow rates, separation between the two streams is complete and little reactant crossover occurs. We have previously demonstrated that various separating electrolyte flow rates achieve similar fuel cell polarization, and concluded that the minimal electrolyte flow rate be used to separate reactants [64].

2. Experimental methods

2.1. Fuel cell construction and characterization

The fuel cell consists of three PMMA layers fabricated using a carbon dioxide laser ablation system (M360, Universal Laser Systems, Scottsdale, AZ). The bottom layer has holes cut out for inserting 0.127 mm sections of platinum wire (SPPL-010, Omega Engineering, Stamford, CT) that serve as current collectors. The wires come in contact with the electrodes which are 1 mm tall and 8 mm long stacked sheets of Toray carbon paper (E-TEK, Somerset, NJ) housed in the middle layer. The distance between the parallel carbon anode and cathode electrodes is 1 mm. The active projected electrode area in the cell is 0.08 cm^2, and all absolute current and power numbers are normalized by this area. The top layer of the fuel cell seals the assembly with holes cut out for fluidic access. Liquids are delivered to the cell using 1.5 mm tubing (Tygon™ EW-06418-02, Cole Parmer, Vernon Hills, IL) bonded to the ports with quick dry epoxy. The three PMMA layers are adhered using double sided adhesive Mylar (3M, St. Paul, MN).

The electrolyte and both reactants are delivered to the fuel cell by two independent programmable syringe pumps (KDS200, KD Scientific, Holliston, MA). Reactant flow rates ranged from 50 to 500 $\mu l\,min^{-1}$, and electrolyte flow rates ranged from 0 to 250 $\mu l\,min^{-1}$. We record polarization data for cell 1 and cell 2 using

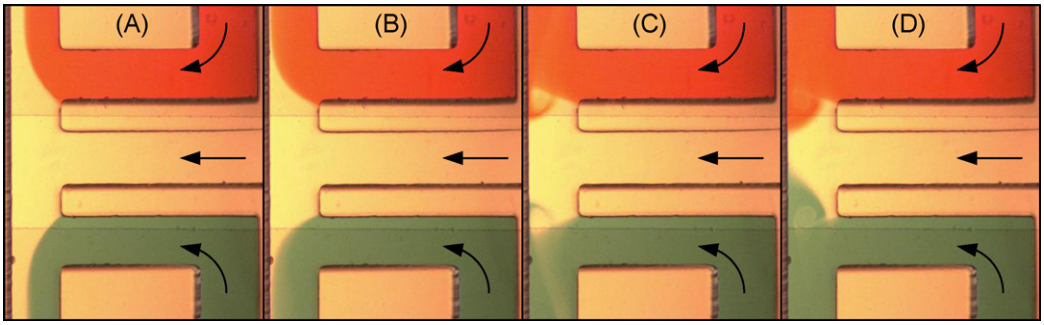

Fig. 2. Optical micrographs showing reactant separation under various flow rate ratios of the reactants (red and blue) to that of the electrolyte (clear) in μl min^{-1}. (A) 50:50, (B) 200:50, (C) 500:50, and (D) 800:50, where 50 μl min^{-1} corresponds to Re = 6. Arrows represent the flow direction, and the channel width is 800 μm. The reactants remain separated even at large Re numbers. (For interpretation of the references to color in this figure legend, the reader is referred to the web version of the article.)

a source meter (Model 2410, Keithley Instruments, Cleveland, OH) and a potentiostat (VersaSTAT 4, Princeton Applied Research, Oak Ridge, TN) respectively. We hold cell 1 at a fixed current density, and then completely polarize cell 2 by galvanostatic steps. We report the average cell 2 voltage after it equilibrates for 10–15 s. We then step the cell 1 current density, and repeat the polarization for cell 2.

2.2. Chemistry

We use vanadium redox species in acidic media (V^{2+}/V^{3+} at the anode and VO_2^+/VO^{2+} at the cathode) to characterize the fuel cell. While vanadium as a fuel exhibits lower energy densities than alcohols or organic acids, its high activity on bare carbon and its high open circuit potential make it an appealing selection for testing new microfluidic fuel cell architectures. We prepare 50 mM V^{2+} and VO_2^+ in 1 M sulfuric acid through electrolysis of VO^{2+}.

Reactants for the cell are obtained by first preparing 50 mM vanadium(IV) oxide sulfate hydrate (CAS 123334-20-3, Sigma Aldrich, St. Louis, MO) in sulfuric acid (CAS 7664-93-9, EMD Chemicals, Hibbstown, NJ) diluted to 1 M in 18.3 MΩ deionized water (Millipore, Billerica, MA). After mixing, a clear blue solution indicates the presence of the vanadium(IV) ion. An in-house electrolytic cell was fabricated using PMMA for the housing, Toray paper for the electrodes, and a Nafion membrane (NRE212, Fuel Cell Store, Boulder, CO) as the ion exchange medium [35]. The electrolytic cell generates the oxidation states vanadium(II) and vanadium(V) from the stock vanadium(IV) [65]. At the cathode of the electrolytic cell the reaction:

$$VO^{2+} + 2H^+ + e^- \leftrightarrow V^{3+} + H_2O, \quad E^o = 0.337\,\text{V vs SHE} \tag{1}$$

occurs, followed by

$$V^{3+} + e^- \leftrightarrow V^{2+}, \quad E^o = -0.255\,\text{V vs SHE} \tag{2}$$

At the anodic half cell the reaction:

$$VO^{2+} + H_2O \leftrightarrow VO_2^+ + 2H^+ + e^-, \quad E^o = 0.991\,\text{V vs SHE} \tag{3}$$

occurs. To obtain V^{2+} as the fuel, the charge balance requires that the anodic half cell of the electrolysis setup be twice the volume of its cathodic counterpart. A nitrogen gas stream is constantly introduced to the cathodic half cell to maintain vanadium(II) stability [34].

At the fuel cell anode the oxidation reaction

$$V^{2+} \leftrightarrow V^{3+} + e^-, \quad E^o = -0.255\,\text{V vs SHE} \tag{4}$$

occurs and at the cathode the reduction

$$VO_2^+ + 2H^+ + e^- \leftrightarrow VO^{2+} + H_2O, \quad E^o = 0.991\,\text{V vs SHE} \tag{5}$$

occurs [65].

3. Results and discussion

In this section we present polarization results for two cells stacked fluidically in series and electrically in parallel and compare it to the performance of a single cell. We also present the effects of reactant and separating electrolyte flow rate on the polarization of each fuel cell in the device, and investigate how the polarization of cell 1 affects that of cell 2. We conclude with a discussion on fuel utilization and overall efficiency of stacked microfluidic fuel cells.

3.1. Stack polarization

The multi-pass fuel cell allows for on-chip reactant recycling and can be analyzed as a single microfluidic fuel cell. It is similar to a PEM stack with bipolar plates in that the reactants pass serially through several reactive zones. We electrically connect cell 1 and cell 2 in parallel, i.e. a common anode and common cathode. When the reactants are subjected to two ion exchange zones the effective cross-sectional area of the fuel cell doubles. This area increase results in an effective reduction in overall Ohmic losses since the fuel cell resistance can be approximated as $R = g/\sigma A$, where g is the length between the electrodes, σ is the conductivity of the solution in the gap, and A is the cross-sectional area of the ion exchange zone. Fig. 3 compares polarization and power density curves between a

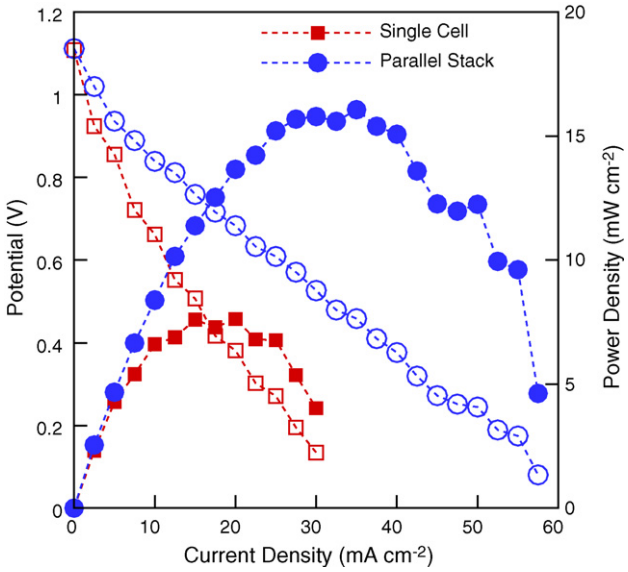

Fig. 3. Polarization and power density curves for single and stacked cell (common anodes, common cathodes) configurations. By doubling the number of interface zones, both the maximum power density and maximum fuel utilization nearly double.

single and the multi-pass microfluidic fuel cells electrically connected in parallel. In this case the reactant and the separating electrolyte flow rates are 500 and 25 μl min^{-1}, respectively. The Ohmic loss differences are distinct between the two cases, where the slope of the linear region of the stacked cell is approximately half that of the single cell. We do not readily observe any curvature in the polarization curves that would typically be associated with activation or mass transport losses. Vanadium redox species exhibit fast electrode kinetics on bare carbon, and at 500 μl min^{-1} mass transport losses are delayed and the majority of the polarization curve reflects the Ohmic losses.

The peak power density (and its respective current density) increases from 7.5 to 16 mW cm^{-2} upon doubling the number of fuel cell passes. The maximum fuel utilization also increases from 6% to 11%, calculated as:

$$\eta = \frac{i \cdot A}{nFCQ} \tag{6}$$

where i is the maximum measured current density, A is the top projected electrode area, n is the number of electrons transferred, F is Faraday's constant, C is the concentration of the fuel, and Q is the fuel flow rate. This design presents the first example of a membraneless microfluidic fuel cell that reuses reactants, in contrast to multichannel systems that employ common manifolds for inlets and outlets, as shown by Hollinger et al. [63].

The vanadium fuel utilization values reported here are lower than large scale, membrane-based [66] and microfluidic membraneless [36] fuel cells, which report utilization values larger than 90%. In this work we are characterizing our architecture using low vanadium concentrations and higher flow rates. Both of these parameters result in decreased reaction rates at the electrode surface, and thus lower fuel utilization. While the fuel concentration and flow rate can be tuned to achieve near complete utilization, the focus of this study is to enable higher power density from larger flow rates and increased fuel utilization from reactant reuse.

3.2. Individual fuel cell polarization

While the primary interest is the power output of the overall stack, it is important to understand how the polarization of one cell in the stack influences that of downstream cells [67,68]. Fig. 4A–C shows polarization data for cell 1 and cell 2 at reactant/electrolyte flow rate ratios of 50/25, 500/250, and 500/25 (in μl min^{-1}), respectively. Cell 2 is downstream of cell 1 and its potential is dependent on the local reactant concentration and flow conditions which are modified by the operation of cell 1; therefore cell 2's polarization is noted as a function of the current density of cell 1 in each figure. Here we detail the effects of reactant and electrolyte flow rate on the potential output of the individual fuel cells.

In all three flow rate cases, we observe lower maximum current densities from cell 2 as we increase the current density from cell 1. For example, in Fig. 4B, cell 2's maximum current density drops from 22.5 to 12.5 mA cm^{-2} when we increase cell 1's current density from zero (open circuit potential) to 20 mA cm^{-2}. We attribute this decrease in cell 2's current density to lower reactant concentrations onset by dilution and utilization from cell 1. Lower reactant concentrations in the fuel cell result in current density losses due to lower reaction rates [69], and Nernstian potential losses due to a decrease in species activity and net Gibbs free energy [70].

The decrease in cell 2's maximum current density due to cell 1 is accentuated at low flow rates. For example, Fig. 4A shows that at the 50 μl min^{-1} reactant flow rate, cell 2's highest current density is approximately 25% of cell 1's current. At high reactant (500 μl min^{-1}) and low electrolyte (25 μl min^{-1}) flow rates shown in Fig. 4C, we observe nearly equivalent maximum current densities from both cell 1 and cell 2 over the entire range of cell 1's current density. At low reactant flow rates, cell 1 uses a larger fraction of the available reactants and results in lower reactant concentrations exiting cell 1. This effect results in a drastic decrease in cell 2's current density with larger cell 1 current densities.

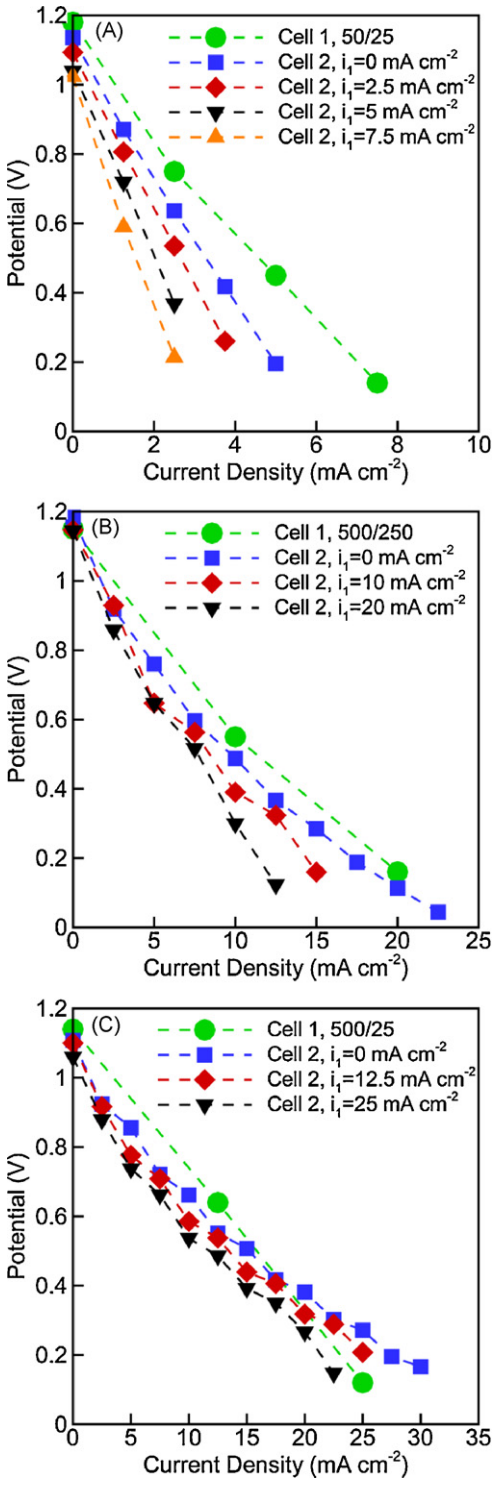

Fig. 4. Polarization curves at (A) 50 μl min^{-1} reactant and 25 μl min^{-1} separating electrolyte flow rate, (B) 500 μl min^{-1} reactant and 250 μl min^{-1} separating electrolyte flow rate, and (C) 500 μl min^{-1} reactant and 25 μl min^{-1} separating electrolyte flow rate. The current density i_1 denoted in the legend reflects the galvanostatic state of cell 1 during cell 2's polarization. In all three cases higher current densities from cell 1 decreases the maximum current density of cell 2.

We also consider the effect of the separating electrolyte flow rate on the individual cell polarization. Fig. 4B and 4C, show that

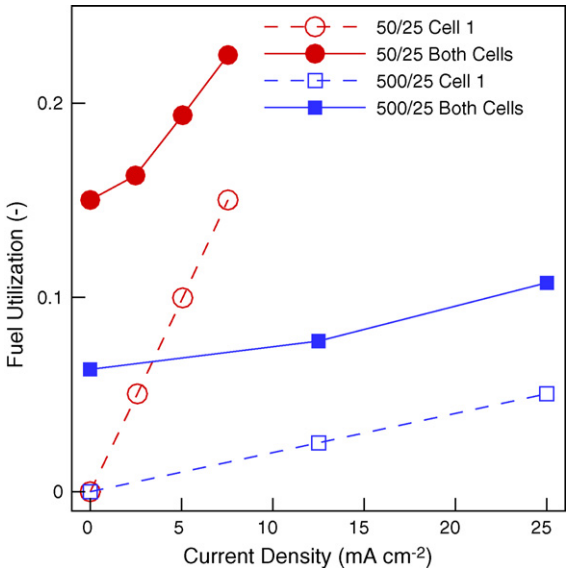

Fig. 5. Comparison of overall fuel utilization for cell 1 (open symbols) and both cells (filled symbols) for 50 μl min^{-1} (●) and 500 μl min^{-1} (■) reactant flow rate. The separating electrolyte flow rate is 25 μl min^{-1}. The increase in fuel utilization is an advantage of recycling the reactants.

we observe very similar polarization curves for cell 1 at the flow rate cases 500/250 and 500/25. Since the reactions occur prior to the three stream interface, the first cell's operation is not dependent on the separating electrolyte flow rate, consistent with our previous findings [64]. However, polarization curves with varying separating electrolyte flow rates are not equivalent in cell 2. At larger separating electrolyte flow rates, we observe a decrease in cell 2's current density with increasing cell 1 current density. For example, comparing Fig. 4B and 4C, we see that cell 2's current density decreases by 5 mA cm^{-2} (at cell 2 = 0.4 V and cell 1 at maximum current density) when higher electrolyte flow rates are used. As the separating electrolyte flow rate increases we expect (i) enhanced mass transport at cell 2's electrode surfaces which results in higher current densities and (ii) decreased reactant availability in cell 2 due to dilution from the added electrolyte which reduces reaction rates and results in lower current densities. From the polarization curves in Fig. 4B and 4C, it is apparent that larger electrolyte flow rates are detrimental to the performance of downstream cells. Under these conditions, the losses due to reactant dilution dominate enhancements of mass transport.

In parallel flow membraneless designs, species mixing by diffusion induces potential losses due to reactant crossover and depletion. In the current architecture the concentration gradients at the interface are aligned with the bulk fluid flow. At each reaction zone reactant diffusion is dependent on the local Peclet (Pe) number, where $Pe = (\nu/D) \times Re$, and (ν/D) is the Schmidt number (ratio of kinematic viscosity to diffusivity), and Re is the Reynolds number. In dilute aqueous solutions, we estimate the Peclet number as $Pe = 1000 \times Re$, and thus our smallest Pe number would approximately equal 6000. We can therefore deduce that cross species diffusion in the reaction zone is small.

3.3. Fuel utilization

We calculate the overall fuel utilization from a two cell system as:

$$\eta_o = \left(\frac{i_1}{nFCQ} + \frac{i_2}{nFCQ}\right) \cdot A \quad (7)$$

Fig. 5 plots the fuel utilization from cell 1 alone as well as the overall fuel utilization using Eq. (7) for the flow rate cases of 50/25 and 500/25. The fuel utilization is plotted as a function of the cell 1 current density and the maximum current from cell 2. We observe that fuel utilization increases linearly with increasing cell 1 current density, consistent with Eq. (7). We also note that the fuel utilization decreases with increasing flow rate, consistent with previous observations [52,63,64]. The maximum fuel utilization from cell 2 – when cell 1 current density is zero (i.e. no fuel is used in cell 1) – is approximately equal to the maximum fuel utilization from cell 1, regardless of the flow rate. This result shows that both cells operate nearly identical if treated individually. The near doubling of power density (Fig. 3) and fuel utilization (solid over open symbols) shown in Fig. 5 is due to equal contributions from both cells. Fig. 5 shows that the fuel utilization for two cells is twice as large as a single cell when high flow rates (500/25) are used. When the lower flow rates are used (50/25), the fuel utilization is larger for two cells than for a single cell. For example, at low flow rates (50/25), the combined fuel utilization at 2.5 mA cm^{-2} is 3.2 higher than the single cell. In contrast, at higher flow rates (500/25) the fuel utilization for the combined cells is approximately twice that of the single cell across all current densities. If we operate at low current densities, higher flow rates reduce the polarization influence from one cell to the next. Fig. 5 suggests that we can increase fuel utilization by increasing the number of passes at high flow rates. In this configuration we can achieve both high fuel utilization and power output from the fuel cell.

4. Conclusions

The performance of parallel flow based laminar flow fuel cells are limited by mass transport boundary layer growth over flat plate electrodes and diffusive broadening at the interface of fuel and oxidant. High flow rates are used in a effort mitigate these challenges but result in wasted reactants that advect out of the system before completely reacting. In this work, we use porous electrocatalysts to maximize reaction surface area and brief ionic interface zones where reactant diffusion and mixing are mitigated. The multi-pass fuel cell design successfully recycles reactants from one cell to the other through the use of multiple interfaces, which increases both the overall fuel cell power and efficiency of the fuel cell. This work represents the first example of reusing reactants using stacked microfluidic fuel cell architectures, analogous to membrane-based stacked fuel cell systems. The influence of one interface on the next is prominent at low reactant flow rates and high current densities. The power of cell 2 decreases with decreasing reactant flow rate, increasing electrolyte flow rate, and increasing upstream cell current density. When the two interfaces are interconnected to form a single cell, we observe that peak power density and fuel utilization is doubled relative to single cell. This design allows independent and uncoupled control over desired potentials and current densities through prescribing a specific number of interfaces.

Acknowledgment

We acknowledge Arizona State University Graduate Fellowship for funding.

References

[1] D. Dunn-Rankin, E.M. Leal, D.C. Walther, Progress in Energy and Combustion Science 31 (2005) 422–465.
[2] C.K. Dyer, Journal of Power Sources 106 (2002) 31–34.
[3] J.D. Morse, International Journal of Energy Research 31 (2007) 576–602.
[4] G.H. Miley, N. Luo, J. Mather, R. Burton, G. Hawkins, L.F. Gu, E. Byrd, R. Gimlin, P.J. Shrestha, G. Benavides, J. Laystrom, D. Carroll, Journal of Power Sources 165 (2007) 509–516.

[5] A.M. Cardenas-Valencia, J. Dlutowski, S. Knighton, C.J. Biver, J. Bumgarner, L. Langebrake, Sensors and Actuators B: Chemical 122 (2007) 328–336.
[6] K.L. Chu, M.A. Shannon, R.I. Masel, Journal of the Electrochemical Society 153 (2006) A1562–A1567.
[7] S. Ha, B. Adams, R.I. Masel, Journal of Power Sources 128 (2004) 119–124.
[8] Y.Q. Jiang, X.H. Wang, L.Y. Zhong, L.T. Liu, Journal of Micromechanics and Microengineering 16 (2006) S233–S239.
[9] A. Kamitani, S. Morishita, H. Kotaki, S. Arscott, Journal of Micromechanics and Microengineering 18 (2008).
[10] B.H. Liu, Z.P. Li, K. Arai, S. Suda, Electrochimica Acta 50 (2005) 3719–3725.
[11] N. Nam-Trung, C. Siew Hwa, Journal of Micromechanics and Microengineering (2006) R1.
[12] K. Shah, W.C. Shin, R.S. Besser, Sensors and Actuators B: Chemical 97 (2004) 157–167.
[13] S.C. Yao, X.D. Tang, C.C. Hsieh, Y. Alyousef, M. Vladimer, G.K. Fedder, C.H. Amon, Energy 31 (2006) 636–649.
[14] J. Yeom, G.Z. Mozsgai, B.R. Flachsbart, E.R. Choban, A. Asthana, M.A. Shannon, R. Kenis, Sensors and Actuators B: Chemical 107 (2005) 882–891.
[15] A. Collier, H.J. Wang, X.Z. Yuan, J.J. Zhang, D.P. Wilkinson, International Journal of Hydrogen Energy 31 (2006) 1838–1854.
[16] F.A. de Bruijn, V.A.T. Dam, G.J.M. Janssen, Fuel Cells 8 (2008) 3–22.
[17] D.A. Schiraldi, Polymer Reviews 46 (2006) 315–327.
[18] W. Schmittinger, A. Vahidi, Journal of Power Sources 180 (2008) 1–14.
[19] H.L. Tang, P.K. Shen, S.P. Jiang, W. Fang, P. Mu, Journal of Power Sources 170 (2007) 85–92.
[20] J. Wu, X.Z. Yuan, J.J. Martin, H. Wang, J. Zhang, J. Shen, S. Wu, W. Merida, Journal of Power Sources 184 (2008) 104–119.
[21] N. Yousfi-Steiner, P. Moçotéguy, D. Candusso, D. Hissel, Journal of Power Sources 194 (2009) 130–145.
[22] J.R. Yu, T. Matsuura, Y. Yoshikawa, M.N. Islam, M. Hori, Physical Chemistry Chemical Physics 7 (2005) 373–378.
[23] C.R. Buie, J.D. Posner, T. Fabian, C.A. Suk-Won, D. Kim, F.B. Prinz, J.K. Eaton, J.G. Santiago, Journal of Power Sources 161 (2006) 191–202.
[24] K.D. Hristovski, B. Dhanasekaran, J.E. Tibaquira, J.D. Posner, P.K. Westerhoff, Journal of Water Supply Research and Technology: Aqua 58 (2009) 327–335.
[25] H. Li, Y.H. Tang, Z.W. Wang, Z. Shi, S.H. Wu, D.T. Song, J.L. Zhang, K. Fatih, J.J. Zhang, H.J. Wang, Z.S. Liu, R. Abouatallah, A. Mazza, Journal of Power Sources 178 (2008) 103–117.
[26] X. Cheng, J.L. Zhang, Y.H. Tang, C.J. Song, J. Shen, D.T. Song, J.J. Zhang, Journal of Power Sources 167 (2007) 25–31.
[27] K.J. Jeong, C.A. Miesse, J.H. Choi, J. Lee, J. Han, S.P. Yoon, S.W. Nam, T.H. Lim, T.G. Lee, Journal of Power Sources 168 (2007) 119–125.
[28] E. Kjeang, J. Goldak, M.R. Golriz, J. Gu, D. James, K. Kordesch, Fuel Cells 5 (2005) 486–498.
[29] S.S. Kocha, J.D.L. Yang, J.S. Yi, AICHE Journal 52 (2006) 1916–1925.
[30] E.R. Choban, L.J. Markoski, A. Wieckowski, P.J.A. Kenis, Journal of Power Sources 128 (2004) 54–60.
[31] R. Ferrigno, A.D. Stroock, T.D. Clark, M. Mayer, G.M. Whitesides, Journal of the American Chemical Society 124 (2002) 12930–12931.
[32] E. Kjeang, N. Djilali, D. Sinton, Journal of Power Sources 186 (2009) 353–369.
[33] E. Kjeang, N. Djilali, D. Sinton, T.S. Zhao, Micro Fuel Cells, Academic Press, Boston, 2009, pp. 99–139.
[34] E. Kjeang, J. McKechnie, D. Sinton, N. Djilali, Journal of Power Sources 168 (2007) 379–390.
[35] E. Kjeang, B.T. Proctor, A.G. Brolo, D.A. Harrington, N. Djilali, D. Sinton, Electrochimica Acta 52 (2007) 4942–4946.
[36] E. Kjeang, R. Michel, D.A. Harrington, N. Djilali, D. Sinton, Journal of the American Chemical Society 130 (2008) 4000–4006.
[37] K.S. Salloum, J.R. Hayes, C.A. Friesen, J.D. Posner, Journal of Power Sources 180 (2008) 243–252.
[38] J.L. Cohen, D.J. Volpe, D.A. Westly, A. Pechenik, H.D. Abruna, Langmuir 21 (2005) 3544–3550.
[39] M.H. Sun, G.V. Casquillas, S.S. Guo, J. Shi, H. Ji, Q. Ouyang, Y. Chen, Microelectronic Engineering 84 (2007) 1182–1185.
[40] J.R. Hayes, A.M. Engstrom, C. Friesen, Journal of Power Sources 183 (2008) 257–259.
[41] S.M. Mitrovski, R.G. Nuzzo, Lab on a Chip 6 (2006) 353–361.
[42] R.S. Jayashree, M. Mitchell, D. Natarajan, L.J. Markoski, P.J.A. Kenis, Langmuir 23 (2007) 6871–6874.
[43] E. Kjeang, A.G. Brolo, D.A. Harrington, N. Djilali, D. Sinton, Journal of the Electrochemical Society 154 (2007) B1220–B1226.
[44] A. Lam, D.P. Wilkinson, J.J. Zhang, Journal of Power Sources 194 (2009) 991–996.
[45] I.B. Sprague, P. Dutta, S. Ha, Proceedings of the Institution of Mechanical Engineers Part A: Journal of Power and Energy 223 (2009) 799–808.
[46] S. Topcagic, S.D. Minteer, Electrochimica Acta 51 (2006) 2168–2172.
[47] J. Ma, Y. Liu, Y. Liu, Y. Yan, P. Zhang, Fuel Cells 8 (2008) 394–398.
[48] E. Kjeang, R. Michel, D.A. Harrington, D. Sinton, N. Djilali, Electrochimica Acta 54 (2008) 698–705.
[49] F.R. Brushett, R.S. Jayashree, W.-P. Zhou, P.J.A. Kenis, Electrochimica Acta 54 (2009) 7099–7105.
[50] F.R. Brushett, W.P. Zhou, R.S. Jayashree, P.J.A. Kenis, Journal of the Electrochemical Society 156 (2009) B565–B571.
[51] E.R. Choban, J.S. Spendelow, L. Gancs, A. Wieckowski, P.J.A. Kenis, Electrochimica Acta 50 (2005) 5390–5398.
[52] R.S. Jayashree, S.K. Yoon, F.R. Brushett, P.O. Lopez-Montesinos, D. Natarajan, L.J. Markoski, P.J.A. Kenis, Journal of Power Sources 195 (2010) 3569–3578.
[53] R.B. Bird, E.N. Lightfoot, W.E. Stewart, Transport Phenomena, 2nd ed., John Wiley and Sons, Inc., New York, NY, 2001.
[54] R.F. Probstein, Physicochemical Hydrodynamics: An Introduction, vol. 2, Wiley, 2003.
[55] E.R. Choban, P. Waszczuk, P.J.A. Kenis, Electrochemical and Solid State Letters 8 (2005) A348–A352.
[56] R.F. Ismagilov, A.D. Stroock, P.J.A. Kenis, G. Whitesides, H.A. Stone, Applied Physics Letters 76 (2000) 2376–2378.
[57] S.K. Yoon, G.W. Fichtl, P.J.A. Kenis, Lab on a Chip 6 (2006) 1516–1524.
[58] A. Bazylak, D. Sinton, N. Djilali, Journal of Power Sources 143 (2005) 57–66.
[59] F.L. Chen, M.H. Chang, M.K. Lin, Electrochimica Acta 52 (2007) 2506–2514.
[60] J. Lee, K.G. Lim, G.T.R. Palmore, A. Tripathi, Analytical Chemistry 79 (2007) 7301–7307.
[61] H.B. Park, D.H. Ahmed, K.H. Lee, H.J. Sung, Electrochimica Acta 54 (2009) 4416–4425.
[62] R.S. Jayashree, L. Gancs, E.R. Choban, A. Primak, D. Natarajan, L.J. Markoski, P.J.A. Kenis, Journal of the American Chemical Society 127 (2005) 16758–16759.
[63] A.S. Hollinger, R.J. Maloney, R.S. Jayashree, D. Natarajan, L.J. Markoski, P.J.A. Kenis, Journal of Power Sources 195 (2010) 3523–3528.
[64] K.S. Salloum, J.D. Posner, Journal of Power Sources 195 (2010) 6941–6944.
[65] D.R. Lide (Ed.), CRC Handbook of Chemistry and Physics, 90th ed., CRC Press/Taylor and Francis, Boca Raton, FL, 2010 (Internet Version 2010).
[66] M. Skyllaskazacos, D. Kasherman, D.R. Hong, M. Kazacos, Journal of Power Sources 35 (1991) 399–404.
[67] A.C. Burt, I.B. Celik, R.S. Gemmen, A.V. Smirnov, Journal of Power Sources 126 (2004) 76–87.
[68] T. Mennola, M. Mikkola, M. Noponen, T. Hottinen, P. Lund, Journal of Power Sources 112 (2002) 261–272.
[69] H.S. Fogler, Elements of Chemical Reaction Engineering, Prentice-Hall, Inc., 1986.
[70] J. Larminie, A. Dicks, Fuel Cell Systems Explained, 2nd ed., John Wiley & Sons Ltd., 2003.